Polymer 49 (2008) 3130–3135

Contents lists available at ScienceDirect

Polymer

journal homepage: www.elsevier.com/locate/polymer

# Cooperative rearranging region size in semi-crystalline poly(L-lactic acid)

N. Delpouve [a], A. Saiter [a], J.F. Mano [b,c], E. Dargent [a,*]

[a] Laboratoire PBS, FRE 3101, LECAP, Institut des Matériaux de Rouen. Université de Rouen, Faculté des Sciences, Avenue de l'Université BP 12, 76801 Saint Etienne du Rouvray, France
[b] 3B's Research Group – Biomaterials, Biodegradables and Biomimetics, Department of Polymer Engineering, Campus de Gualtar, 4710-057 Braga, Portugal
[c] IBB – Institute for Biotechnology and Bioengineering, Braga, Portugal

ARTICLE INFO

*Article history:*
Received 25 January 2008
Received in revised form 1 April 2008
Accepted 23 April 2008
Available online 30 April 2008

*Keywords:*
Poly(L-lactic acid)
CRR
Glass transition

ABSTRACT

The amorphous phase geometrically confined at the nanometric length scale in semi-crystalline polymers exhibits different conformational dynamics with respect to the pure amorphous situation. In this work, we have studied the influence of the crystalline phase on the structural relaxation phenomena occurring in the amorphous phase by characterizing the cooperative rearranging region (CRR) in poly(L-lactic acid), PLLA, a well known biodegradable polyester. More particularly, the evolution of the characteristic cooperativity length $\xi_{T_g}$ at the glass transition is investigated in function of the crystallinity degree using Temperature Modulated Differential Scanning Calorimetry, TMDSC. Thermal analyses have been performed on PLLA cold crystallized at 80 °C for different durations in order to obtain a crystallinity degree varying between 0 and 42%. We show that two types of mobile amorphous phases exist: the amorphous matrix and the amorphous fraction trapped in the spherulites. For this latter one, a clear confinement effect is shown despite the fact that the amorphous domain size is larger than $\xi_{T_g}$. This behavior is attributed to the chemical connection between the mobile and the rigid fraction of the polymer.



## 1. Introduction

In the vitreous polymer amorphous phase, relaxation processes are known to be cooperative phenomena and the molecule motions depend on neighbor's motions [1]: The rearranging movement of one structural unit is only possible if a certain number of neighboring structural units is also moved. Adam and Gibbs [2] introduced the notion of cooperative rearranging region (CRR) defined as a subsystem, which can rearrange its configuration into another, independently of its environment upon a sufficient thermal fluctuation. If the total volume of a system is divided into equal "Adam–Gibbs volumes", the density $\rho$, the temperature $T$, the entropy $S$, and the energy $E$ are somewhat different in each subvolume, and the mean square fluctuations $\langle\Delta\rho^2\rangle$, $\langle\Delta T^2\rangle$, $\langle\Delta S^2\rangle$, and $\langle\Delta E^2\rangle$ are given by standard relations of statistical thermodynamics [3]. The main idea of Donth et al. [4–6] was to relate these statistical thermodynamic relations to the width of relaxation time distribution of the so-called $\alpha$ process. Each subvolume (called also CRR) with a specific size equal to $V_{SV}=\xi^3$ can be then considered as a thermodynamic system in metastable equilibrium with fluctuating variables having a Gaussian distribution. Each subvolume has its own glass transition temperature $T_g$ and its own relaxation time $\tau$. In this theory the relaxation time distribution is related to the glass transition distribution where $\langle T_g\rangle$ is assumed to be the conventional glass transition of the sample. According to Donth's approach [7], the characteristic volume of cooperativity at $T_g$ noted $\xi^3_{T_g}$, can be estimated from the following equation:

$$\xi^3_{T_g} = \frac{\Delta(1/C_v)}{\rho(\delta T)^2} k_B T_g^2 \quad (1)$$

where $\delta T$ the mean temperature fluctuation related to the dynamic glass transition of one CRR [7–9], $T_g$ the glass transition temperature, $k_B$ the Boltzmann constant, $\rho$ the polymer density and $C_v$ the heat capacity at constant volume. The approximation for the calculation of the characteristic cooperativity volume $\xi^3_{T_g}$ from Eq. (1) neglects the difference between the heat capacity step at constant pressure and at constant volume, and the step of reciprocal specific heat capacity can be estimated from:

$$\Delta(1/C_v) \approx \Delta(1/C_p) = (1/C_p)_{glass} - (1/C_p)_{liquid} \quad (2)$$

The average size of each subvolume called cooperative rearranging region (CRR) can be estimated from Temperature Modulated Differential Scanning Calorimetry, TMDSC, for example. Many recent works on the determination of the CRR size according to Donth's approach exist in the literature [10–13]. One of them [12] shows the influence of geometrical confinement on the CRR size in syndiotactic poly(methyl methacrylate) system and proves that the

* Corresponding author. Tel.: +332 32 95 50 83; fax: +332 32 95 50 82.
*E-mail address:* eric.dargent@univ-rouen.fr (E. Dargent).

0032-3861/$ – see front matter © 2008 Elsevier Ltd. All rights reserved.
doi:10.1016/j.polymer.2008.04.045

CRR average size decreases when the polymeric matrix is more and more constrained by layers.

This discussion may be inserted in the general problem dealing with the material behavior geometrically confined on a nanometer spatial scale, such as 3D confinement (in nanoporous glasses or zeolites for example), 2D confinement (in silicate layers of nanocomposites or in layered block copolymers) or thin polymer films. The understanding of the finite-size effects on the material properties may be also relevant for technological reasons in areas such as chemical engineering, biomaterials, medicine, microelectronics and a series of applications in nanotechnologies [14–16].

The geometrical confinement exists in semi-crystalline polymers, where a material amorphous phase is placed within the spherulitic structures. Consensus seems now to be reached that at least three different regions must be considered to describe semi-crystalline structure [17]. A three phase model is used to explain the material nano-organization [18], where a non-oriented nanophase called rigid amorphous fraction (RAF) which does not contribute to the glass transition event is considered between the mobile amorphous phase and the crystalline lamellae. The mobile amorphous layer is two-dimensionally confined between two of such layers. Therefore, semi-crystalline systems may also be used as an adequate model to study conformational mobility in confined geometries. Poly(ethylene terephthalate), PET, and other polyesters, have been widely used in this context. Using different thermal histories Hong et al. [19] prepared different microstructures in poly(trimethylene terephthalate) in order to induce different thickness in the mobile amorphous part placed between the crystalline lamellae, $L_{ma}$ that varied between 2.6 and 1.7 nm. The cubic root of the CRR volume called $\xi_{T_g}$ decreased in the range of 2.5 and 1.9 nm when $L_{ma}$ decreased, reflecting the higher degree of confinement. The $\xi_{T_g}$ values are typical from what is reported in the literature, and in this particular case they are of the same order of magnitude of $L_{ma}$. The $L_{ma}$ values are also quite small in PET, in the range of 3.3–1.8 nm [20].

In order to study if some long order distance in confinement could influence the CRR size, other systems exhibiting higher $L_{ma}$ values would be interesting. In a previous study it was found that upon different thermal treatments poly(L-lactic acid), PLLA, presents $L_{ma}$ values could be higher than 6.0 nm, i.e. higher than the usual $\xi_{T_g}$ values [21]. Therefore, the main goal of the present work is to correlate crystallinity degree (and the corresponding $L_{ma}$ values) and CRR size in PLLA. This study could be useful to complete other works dealing with the crystalline morphology effect on the glass transition dynamics [21–25]. Moreover, it was seen before that for intermediate crystallinity levels both processes could be observed by DSC, provided that the samples were annealed below $T_g$ [31]; this procedure allowed to detect the processes in a more clear way as the glass transition events were observed as endothermic peaks during heating, as a result of the enthalpy recovery. In this work an attempt will be made to identify and separate the two glass transition processes using TMDSC, without previously aging the samples.

## 2. Experimental

The poly(L-lactic acid) (PLLA) used in this work is of high stereoregularity and was provided by Cargill–Dow. The number-average molecular weight is $M_n = 69\,000$ g/mol, polydispersity is 1.73 and it was estimated to have a L-lactide content of 99.6%. Samples are obtained by the following procedure: at first, a sample is heated in a standard DSC apparatus (DSC7 of Perkin Elmer) at 458 K (above the fusion temperature) for 10 min and cooled as quick as possible ($\approx$50 K/min) to obtain a sample as amorphous as possible. Indeed, in this DSC apparatus the cooling rate is controlled and high enough to avoid noticeable crystallization in PLLA. Then, the sample is cold crystallized at a temperature $T_a$ equal to 353 K (20 K above the glass transition temperature) for a duration time $t_a$ included between 0 and 300 min, and rapidly cooled down to 293 K. Before any TMDSC investigations the sample is heated at 10 K/min from 293 K up to a temperature above the glass transition range in order to erase the thermal history, and cooled at 10 K/min up to 293 K. Finally, the sample can be analyzed by TMDSC performed on a TA apparatus (DSC 2920 CE). The specific heat capacities for each sample with different crystallinity degree were measured using sapphire as a reference. The sample masses have been chosen to be similar of the sapphire sample mass, i.e. approximately 20 mg. The TMDSC experiments are performed with an oscillation amplitude of 0.318 K, an oscillation period of 60 s and with a heating rate of 2 K/min. From TMDSC, different signals can be obtained: the heat flow, from which the crystallinity degree is calculated and the apparent complex heat capacity $C_p^*$. From the ratio between the amplitude of the modulated heat flow $A_q$ and the amplitude of the heating rate $A_\beta$, it is possible to extract $C_p^*$ according to Eq. (3):

$$\left|C_p^*\right| = \frac{A_q}{A_\beta} \times \frac{1}{m} \tag{3}$$

where $m$ is the sample mass. Due to the phase lag $\phi$ between the calorimeter response function (i.e. the heat flow) and the time derivative of the modulated temperature program, two components (the in-phase and out-of-phase components of the apparent complex heat capacity) noted, respectively, $C_p'$ and $C_p''$ can be calculated according to the following equations:

$$C_p' = \left|C_p^*\right| \cos\phi \tag{4}$$

$$C_p'' = \left|C_p^*\right| \sin\phi \tag{5}$$

More details concerning the apparent complex heat capacity determination, especially the measured phase angle correction for contributions originating from heat transfer, are given in Ref. [26]. The $C_p'$ vs. temperature variations appear usually as an endothermic step and the $C_p''$ variations show a peak in the glass transition temperature region. The $C_p''$ peak maximum temperature is called $T_\alpha$ and corresponds to the glass transition temperature $T_g$ in this work. From $C_p'$ and $C_p''$, $\Delta(1/C_p)$ and $\delta T$ values are estimated, respectively, and the CRR average size is calculated.

Structural information is acceded by small-angle X-ray scattering, SAXS, using synchrotron radiation (transmission mode) at the Soft Condensed Matter A2 beamline at HASY(DESY) synchrotron facility in Hamburg (Germany). A Marccd detector is placed 284 cm from the sample, and a radiation with a wavelength of $\lambda = 0.15$ nm is employed. The calibration is performed using well crystallized PET. Polarized light microscopy (Nikon Optiphot-2) with a hot stage (Mettler FP 82 HT) allows to observe the appearance of spherulites (20 μm radius) following the same thermal cycle than DSC. Pictures are taken at the temperature $T_a$ for various time $t_a$.

## 3. Results

The heat flow vs. temperature signals are shown in Fig. 1 for some of samples previously annealed at $T_a = 353$ K, for different times included between 0 and 300 min. Four thermal phenomena are observable for a non-annealed sample ($t_a = 0$ min): an endothermic heat flow step around 333 K characterizing the glass transition, an exothermic peak around 363 K due to the cold crystallization of an amorphous phase part, a weak endo- or exothermic peak at 418 K and finally an endothermic peak around 440 K due to the crystalline phase fusion. An extensive work on PLLA samples

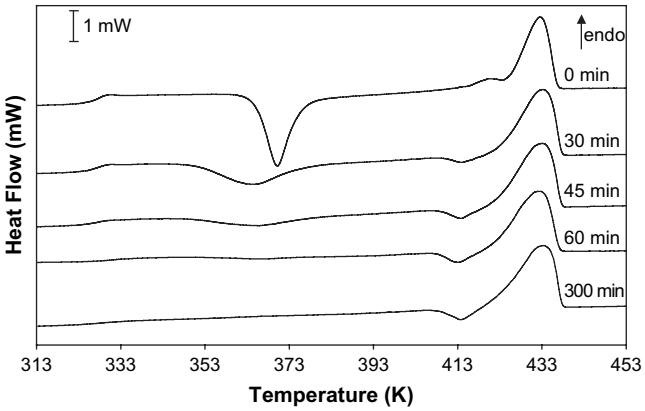


**Fig. 1.** Examples of heat flow curves vs. temperature obtained on PLLA samples annealed at $T_a = 353$ K for different annealed times noted $t_a$ and indicated on the figure.

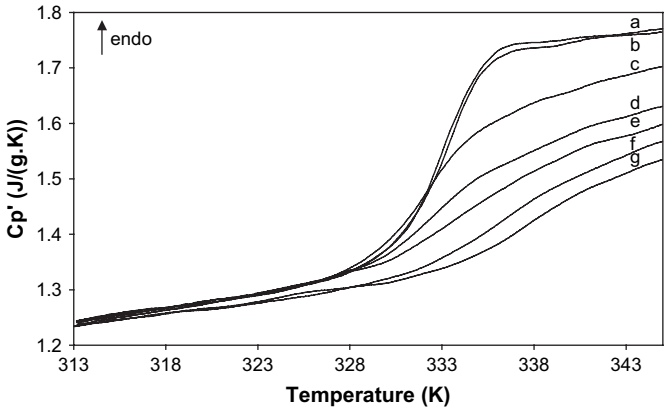


**Fig. 3.** $C_p^*$ in-phase component spectra noted $C_p'$ obtained during heating of PLLA annealed at 353 K during different times: (a) 0 min, (b) 30 min, (c) 35 min, (d) 45 min, (e) 60 min, (f) 90 min, (g) 300 min.

crystallized from the glassy state [27] has shown that, for similar experimental conditions than in this work, the only crystal form observed is the α-phase [28] and at temperatures just below the melting peak, melting and recrystallization of unstable crystals take place almost simultaneously [29]. The melt–recrystallization phenomena could occur between the cold crystallization and the final melting depending on the heating rate [21,30]. For samples annealed between 30 and 60 min, the cold crystallization peak is weaker than for short $t_a$. For samples annealed during time above 60 min, the experimental curve looks different: the glass transition appears with a very weak magnitude and the cold crystallization peak has disappeared. So, the crystalline phase which melted around 440 K has been generated during the annealing. The crystallinity degree $X_c$ induced by the annealing could be deduced from the heat flow curve obtained by TMDSC using the following equation:

$$X_c = \frac{\Delta H_f - \sum \Delta H_c}{\Delta H_f^0} \quad (6)$$

in which $\Delta H_f$ is the measured fusion enthalpy, $\Delta H_f^0$ is the calculated fusion enthalpy of a wholly crystalline material ($\Delta H_f^0 = 93$ J/g [31]) and $\Sigma\Delta H_c$ is the sum of the exothermic peak enthalpies obtained during the TMDSC runs. The crystallinity degree values are reported in Fig. 2. As expected, the $X_c$ variations vs. time are quasi sigmoidal. For small annealing time, a wholly amorphous sample can be obtained by the procedure used in this work; this was confirmed by Wide Angle X-ray Diffraction analysis (not shown here). The crystallinity degree remains negligible for annealing times $t_a$ lower than 20 min. Then, $X_c$ sharply increases from 30 to 60 min to reach finally a value closed to 42%, the maximum crystallinity degree obtained here. Polarized light microscopy allows to observe the appearance of spherulites (20 μm radius) for times included between 30 and 60 min (see pictures in Fig. 2 for two annealing times $t_a$).

We now focus on the glass transition region and more particularly on the CRR average size determination obtained from $C_p'$ and $C_p''$ TMDSC spectra. Fig. 3 gives the $C_p'$ evolution as a function of the annealing time $t_a$. A classical behavior is observed, i.e. a decrease of the $C_p'$ step at the glass transition when the annealing time increases. Indeed, the greater the crystallinity degree, the lower the response of the amorphous phase as the corresponding mass of this component decreases. A shift of the glass transition temperature taken at the middle point $T_{gmid}$ toward higher temperature is also observable. The values vary from 333 to 337 K when the annealing time varies from 0 to 300 min. The $C_p''$ peaks are shown in Fig. 4 for some annealing times $t_a$. For $t_a = 0$ and 30 min, the peaks look similar with $T_\alpha \sim 334$ K, but for $t_a = 35$ and 45 min, the $C_p''$ variations are more complex and a peak with a shoulder at higher temperature is observable. Only a broad peak with $T_\alpha \sim 340$ K is present in the curves for $t_a$ greater than 60 min. The peak magnitude decrease with the annealing time increase is attributed to the relative crystalline phase quantity increase.

Insights at the nanoscale level may be achieved by SAXS allowing to extract information about the lamellar morphology for the case of semi-crystalline polymers. Fig. 5 shows the SAXS pattern of the fully crystallized sample, as a function of the scattering vector. The observed peak is associated with the periodicity

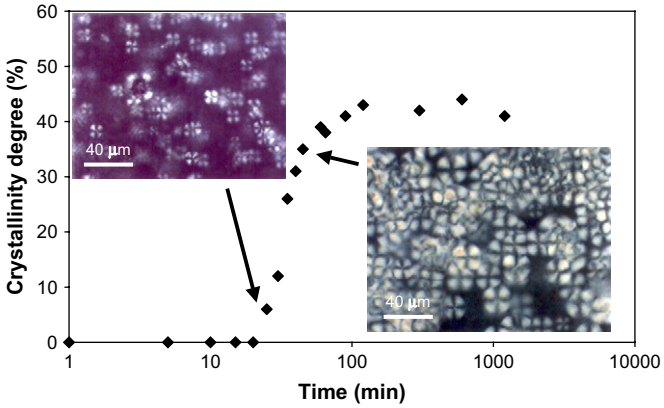


**Fig. 2.** Crystallinity degree variations $X_c$ as a function of the annealing time obtained for PLLA samples annealed at 353 K. The pictures correspond to annealed samples for $t_a$ closed to 30 and 45 min, respectively.

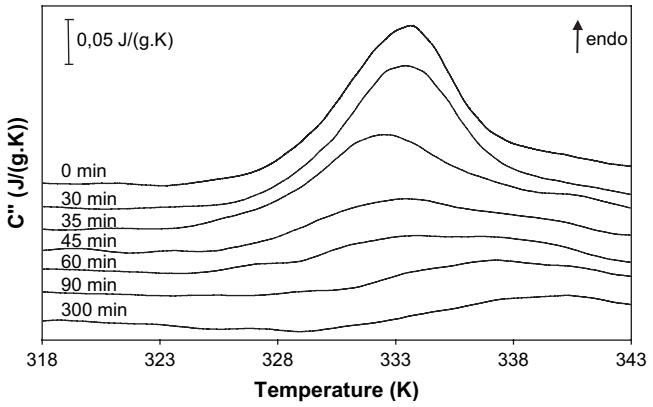


**Fig. 4.** $C_p^*$ out-of-phase component spectra noted $C_p''$ obtained during heating on PLLA annealed at 353 K during different times varying from 0 to 300 min.

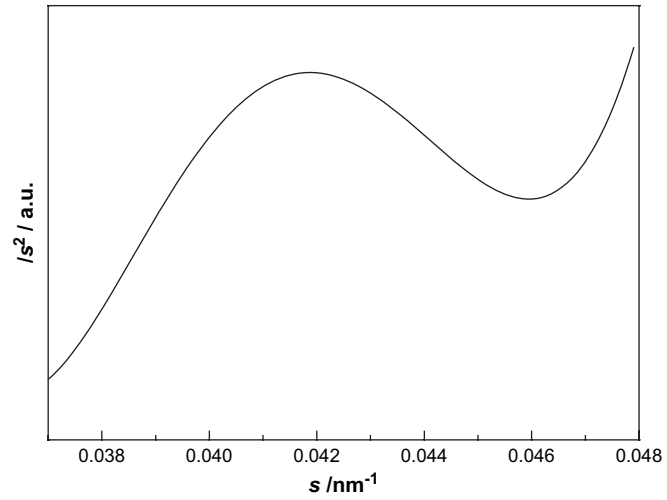


**Fig. 5.** Lorentz-corrected small-angle X-ray scattering of fully crystallized PLLA.

observed in the lamellar structure, and is consistent with results previously obtained [21,31]. The long spacing is calculated by $L = 1/s_{max}$, where $s_{max}$ is the scattering vector of the maximum intensity of the scattering curve. In this case, $L$ is estimated as 23.3 nm. Such value is consistent with data obtained in PLLA samples crystallized at different temperatures $T_a$ where $L$ decreases from 40 down to 24 nm when $T_a$ decreases from 443 down to 383 K [21]. Note that in the present work $T_a = 353$ K.

## 4. Discussion

The $C'_p$ step magnitude decrease is attributed to a decrease of the amorphous phase quantity. Typically, the amorphous phase fraction $X_{ma}$ is calculated from the $\Delta C_p$ step data at the glass transition:

$$X_{ma} = \frac{\Delta C_p}{\Delta C_{p0}} \tag{7}$$

where $\Delta C_p$ is the heat capacity step at $T_g$ for an annealed sample, and $\Delta C_{p0}$ for a 100% amorphous one. As our quenched samples controlled by DSC and X-ray diffraction are fully amorphous, the $\Delta C_{p0}$ value is carefully measured and is equal to 0.48 J $g^{-1}K^{-1}$. The $X_{ma}$ values are reported in Table 1 and it appears $(X_{ma} + X_c)$ lower than 100%, inducing PLLA does probably not follow a two phase model behavior with a crystalline phase and an amorphous one. The deviation from the two phase model is weak for low $X_c$ (0 and 5%) and could be in a first approach attributed to uncertainty or to tiny nucleus of crystalline phase not detected by DSC. Some authors propose to use $^{13}C$ NMR experiments for an accurate determination of the amorphous and crystalline fractions in molecular materials [32]. Nevertheless, deviation from the two phase model is not constant and increases with $X_c$ increasing. These results are consistent with those observed on aromatic polyesters like PET [22] in which $(X_{ma} + X_c)$ is significantly lower than 100%. The rigid amorphous fraction (RAF) [33] noted $X_{ra}$ is deduced from $X_{ma} + X_c + X_{ra} = 100\%$, and the values are reported in Table 1. For semi-crystalline PLLA, the RAF is initially low comparing to other polyesters like PET [22] but increases progressively with $X_c$ increasing until 25%. Indeed, this fraction surrounds the crystals, acting as a link between the crystalline and mobile amorphous phases. As a consequence, the RAF presence limits the mobile amorphous domain size [34].

In the following the discussion concerns the non-crystalline fraction participating to the glass transition, i.e. the mobile amorphous phase (MAP). In order to estimate the CRR average size at the glass transition, $\Delta(1/C_p)$ is determined using Eq. (2), and $(1/C_p)_{glass}$ and $(1/C_p)_{liquid}$ values are estimated from $C'_p$ spectra normalized to the mobile amorphous phase quantity. Indeed, only the MAP participates to the structural relaxation process at the glass transition and is concerned by the CRR concept. From Eq. (1), the average CRR sizes are calculated by taking $\rho = 1.25$ g/cm$^3$ for the PLLA amorphous phase and the temperature fluctuation $\delta T$ is the half-width at half-height of the $C''_p$ spectra. First, we focus on amorphous and highly crystallized samples. For amorphous sample, $\delta T$ is easily determined (2.9 K) and the characteristic cooperativity length value $\xi_{T_g} = 2.9$ nm is reported in Table 1 for $t_a = 0$ min. The same values are obtained for other amorphous sample ($t_a < 30$ min). For fully crystallized samples ($t_a > 60$ min), the peaks are wide and $\delta T$ is closed to 5 K. The characteristic cooperativity length value is closed to $\xi_{T_g} = 2$ nm which is well below the value obtained for amorphous PLLA. We propose to explain such variations between amorphous and semi-crystalline parameters by the existence of two types of mobile amorphous phases in PLLA: an inter-spherulitic amorphous phase and an intra-spherulitic amorphous one. We suppose the relaxation phenomena occur at the glass transition in relatively great CRR ($\xi^3_{T_g} = 27$ nm$^3$) in the PLLA amorphous phase. At the opposite, the intra-spherulitic phase is confined and linked to the crystalline phase thought the RAF and the relaxation phenomena occur at the glass transition in drastically reduced CRR size ($\xi^3_{T_g} = 8$ nm$^3$). This model agrees with observations obtained from different techniques [24,25,35]. Indeed, most of these studies showed that a complex relaxation phenomenon could occur at $T_g$: for intermediate crystallinity degrees two endothermic peaks assigned to enthalpy recovery could be detected, indicating of two distinct glass transition dynamics. This behavior was attributed to a different relaxation mechanism in the inter- and intra-spherulitic amorphous phases. The low temperature process is assigned to the segmental motions within inter-spherulitic amorphous phase and the high temperature process should be assigned to the presence of intra-spherulitic amorphous phase. We must precise that the intra-spherulitic amorphous phase cannot be compared to the RAF. The glass transition of the intra-spherulitic amorphous phase is observed in the glass transition temperature domain (5 K above the response of the amorphous matrix). For semi-crystalline polymers,

**Table 1**
Experimental parameters obtained on PLLA annealed at 353 K for annealed time $t_a$ between 0 and 300 min

| $t_a$ (min) | $X_c$ (%) | $X_{ma}$ (%) | $X_{ra}$ (%) | $T_{gmid}$ (K) | $\Delta(1/C_p)$ (J$^{-1}$ g K) | $\delta T_1$ (K) | $\delta T_2$ (K) | $T_{\alpha 1}$ (K) | $T_{\alpha 2}$ (K) | $\xi_{T_{g1}}$ (nm) | $\xi_{T_{g2}}$ (nm) | Ratio peak1/peak2 |
|---|---|---|---|---|---|---|---|---|---|---|---|---|
| 0 | 0 | 100 | 0 | 333.0 | 0.192 | 2.9 | / | 333.7 | / | 3.0 | / | 100/0 |
| 30 | 12 | 83 | 5 | 333.0 | 0.189 | 2.8 | 3.0 | 333.5 | 340.4 | 3.1 | 3.0 | 86/14 |
| 35 | 26 | 67 | 7 | 332.1 | 0.174 | 3.0 | 4.6 | 332.6 | 339.2 | 2.9 | 2.2 | 62/38 |
| 45 | 35 | 52 | 13 | 332.5 | 0.147 | 3.1 | 4.4 | 332.6 | 338.1 | 2.7 | 2.1 | 46/54 |
| 60 | 39 | 46 | 15 | 334.0 | 0.133 | 2.9 | 4.3 | 332.2 | 337.7 | 2.7 | 2.1 | 25/75 |
| 90 | 41 | 40 | 19 | 336.4 | 0.132 | / | 5.3 | / | 338.3 | / | 1.8 | 0/100 |
| 300 | 42 | 33 | 25 | 337.4 | 0.149 | / | 5.0 | / | 339.7 | / | 2.0 | 0/100 |

$X_c$: crystallinity degree, $X_{ma}$: mobile amorphous phase fraction, $X_{ra}$: rigid amorphous phase fraction, $T_{gmid}$: mid-point glass transition temperature taken on the $C'_p$ curve, $\Delta(1/C_p)$ the step of reciprocal specific heat capacity, $\delta T$: Mean temperature fluctuation, $T_\alpha$: $C''_p$ peak maximum temperature, $\xi_{T_g}$: CRR characteristic length. $\delta T$, $T_\alpha$ and $\xi_{T_g}$ are given for peak P1($t_a$) and P2($t_a$) which fit the low and the high contribution of the $C''_p$ peak, respectively.

the temperature for which the RAF devitrifies is still in debate but Sargsyan et al. suggests that devrification occurs at very higher temperature than the glass transition [36].

The $C_p''$ spectra vs. temperature look sometimes complex which impeded simple extraction of $\delta T$. These spectra show one peak for $t_a < 30$ min and for $t_a > 60$ min (see Fig. 4), and look bimodal for $30 < t_a \leq 60$ min. These annealing times correspond to the spherulite appearance in the amorphous phase. So, we suppose that the amorphous phase response is the sum of intra-spherulitic and bulk-like phase responses. As the consequence, a $\delta T$ value cannot be extracted directly for intermediate $t_a$.

As shown in Fig. 6 for $t_a = 35$ min, we have fitted the experimental curve by a curve $P(t_a)$ which is the sum of two Gaussian curves called $P1(t_a)$ and $P2(t_a)$: $P(t_a) = x \cdot P1(t_a) + y \cdot P2(t_a)$ with $x + y = 1$. These curves $P1(t_a)$ and $P2(t_a)$ are initially P1 (0 min) and P2 (300 min) fitting the $C_p''$ peaks for $t_a = 0$ min or $t_a = 300$ min, respectively, and progressively adjusted to give the best fit. The $P1(t_a)$ and $P2(t_a)$ parameters are reported in Table 1 and used to obtain the CRR parameters. The ratio reported in Table 1 is $100x/100y$. As an example, for $t_a = 35$ min, the fit leads to a ratio of 62/38 indicating the MAP is composed of 62% of bulk-like amorphous phase and 38% of MAP localised in the spherulites. So, below $t_a = 30$ min, the amorphous phase behaves as the bulk-like one, for $30 < t_a \leq 60$ min, the MAP exists in two forms, while for $t_a$ above 60 min the crystallization is maximum and only the intra-spherulitic MAP exists.

When the spherulites grow and emerge from the amorphous phase, the CRR average size, $\xi_{T_{g1}}$ remains constant and the value is $2.9 \pm 0.2$ nm. If we don't take into account the value of $\xi_{T_{g2}}$ for $t_a = 30$ min (this value concerns only 14% of the MAP), we can suppose that the CRR size of the intra-spherulitic MAP is also constant during the spherulites growth and equal to $2 \pm 0.2$ nm. The correlation between an amorphous phase constrained by different factors (crystalline phase, nanoparticles, etc.) and the CRR average size decrease has been already observed in different polymeric systems [37]. Some studies showed that the more constrained the amorphous phase, the smaller the CRR average size [12,38]. The $T_\alpha$ and $\delta T$ differences between $P1(t_a)$ and $P2(t_a)$ (see Table 1) confirm that the crystalline phase influences the amorphous one. Donth et al. [4–6] relate the mean temperature fluctuation $\delta T$ to the width of relaxation time distribution of the glass transition process. Here, we clearly show that the $\delta T$ value increases for intra-spherulitic MAP, meaning the relaxation time distribution width increases when crystalline phase appears. According to our results, it appears that classical parameters characterizing the amorphous phase as $T_g$ and $\Delta C_{p(T_g)}$, are not the only parameters sensitive to the crystalline phase presence in amorphous phase. Indeed, $\delta T$, $T_\alpha$, $\xi_{T_g}$ are directly influenced by the crystalline phase.

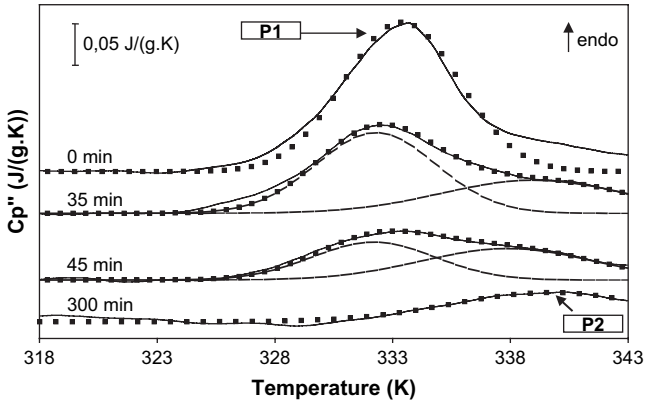


**Fig. 6.** $C_p^*$ out-of-phase component spectra noted $C_p''$ for different durations $t_a$ are drawn in full line. The dashed lines are the Gaussian curves $P1(t_a)$ and $P2(t_a)$. The black squares are the fits $P(t_a)$. P1 is the fit for $t_a = 0$ min and P2 is the fit for $t_a = 300$ min.

From the long period obtained by SAXS it is possible to estimate the thickness of the amorphous layer in fully crystallized sample by $L_{ma} = L \cdot X_{ma} = 9.2$ nm. Such values are substantially higher than the ones found in more studied semi-crystalline polymers, such as PET and PTT [19,20], and also more than three times higher the $\xi_{T_g}$ values obtained in this work. Nevertheless, a clear confinement is found, well expressed by a clear $T_\alpha$ increase and a $\xi_{T_g}$ decrease from 2.9 down to 2.0 nm, upon fully crystallization. Therefore, the results suggest that the strong decrease of $\xi_{T_g}$ should be associated with more than a pure geometrical effect. For the particular case of semi-crystalline polymers, the segments in the inter-crystalline mobile amorphous layer are chemically connected to the rigid interface. These covalent linkages are oriented normally to the surface, inducing the formation of a more ordered/compact amorphous arrangement in the amorphous phase. Note that it was found in a previous paper [39] that the amorphous halo in the wide angle X-ray scattering profile in semi-crystalline PLLA shifts to shift toward higher $2\theta$ values as compared with the amorphous counterpart, indicating that the characteristic distance between the molecular entities is smaller in the crystallized material, and suggesting an intermolecular densification. Such bulk amorphous phase structural modification may also contribute to a $T_g$ and $T_\alpha$ increase and could also influence $\xi_{T_g}$ values.

## 5. Conclusions

From $C_p''$ data, we have shown that the amorphous phase response is different for a wholly amorphous and a semi-crystalline PLLA samples. The two amorphous phases are different to the rigid amorphous fraction which does not contribute directly for the glass transition occurrence. The spherulite emergence leads to the inter-spherulitic amorphous phase decrease and to the intra-spherulitic amorphous phase emergence, having different characteristics: $\xi_{T_g} = 3.0$ nm, $T_\alpha = 333$ K, for the first, and $\xi_{T_g} = 2.0$ nm, $T_\alpha = 338$ K, for the second. SAXS data show that the amorphous layer thickness is substantially higher than $\xi_{T_g}$ ($L_{ma}$ closed to 9 nm). So, the difference in the glass transition dynamic parameters could not be attributed to a simple geometrical confinement effect induced by the crystalline lamellae presence. It is suggested that the amorphous segments chemically linked to the crystalline lamellae enhance the confinement effect. During the spherulite growth, no significant variation of the intra-spherulitic MAP parameters is observed. Therefore, the total conformational dynamics in partially crystallized PLLA, as seen by TMDSC, could be given by a simple linear combination of the two extreme cases: bulk-like amorphous phase case (observed in fully amorphous polymer) and intra-spherulitic amorphous phase (observed in fully transformed polymer).

## Acknowledgments

This work was partially supported by FCT, through the project POCTI/FIS/61621/2004.

## References

[1] Glarum SH. J Chem Phys 1960;33:639.
[2] Adam G, Gibbs JH. J Chem Phys 1965;43:139.
[3] Landau LD, Lifshitz EM. Statistical physics. Reading, MA: Addison-Wesley; 1969.
[4] Donth E. J Non Cryst Solids 1991;131–133:204.
[5] Moynihan CT, Schroeder J. J Non Cryst Solids 1993;161:148.
[6] Mohanty U. Adv Chem Phys 1995;89:89.
[7] Donth E. J Non Cryst Solids 1982;53:325.
[8] Donth E. J Polym Sci B 1996;34:2881.
[9] Donth E. Acta Polym 1999;50:240.
[10] Xia H, Song M. Thermochim Acta 2005;429:1.

[11] Dlubek G. J Non Cryst Solids 2006;352:2869.
[12] Tran TA, Saïd S, Grohens Y. Composites Part A 2005;36:461.
[13] Saiter A, Couderc H, Grenet J. J Therm Anal Calorim 2007;88:483.
[14] Drake JM, Grest GS, Klafter J, Kopelman R, editors. Dynamics in small confining systems IV. Mater Res Soc Symp Proc, vol. 543. Pittsburg PA: Materials Research Society; 1998.
[15] 1st international workshop on dynamics in confinement. In: Frick B, Zorn R, Buttner H, editors. J Phys IV, 10; 2000. p. 7.
[16] Frick B, Koza M, Zorn R. 2nd international workshop on dynamics in confinement. Eur Phys J E 2003;12(1):3–4.
[17] Dlubek G, Gupta AS, Pionteck J, Habler R, Krause-Rehberg R, Kaspar H, et al. Polymer 2005;46:6075.
[18] Wunderlich B. Macromol Rapid Commun 2005;26:1521 and references cited therein.
[19] Hong PD, Chuang WT, Yeh WJ, Lin TL. Polymer 2002;43:6879.
[20] Dobbertin J, Hensel A, Schick C. J Therm Anal 1996;47:1027.
[21] Wang Y, Funari SS, Mano JF. Macromol Chem Phys 2006;207:1262.
[22] Arnoult M, Dargent E, Mano JF. Polymer 2007;48:1012.
[23] Mano JF, Gómez Ribelles JL, Alves NM, Salmerón Sanchez M. Polymer 2005;46:8258.
[24] Dionísio M, Viciosa MT, Wang Y, Mano JF. Macromol Rapid Commun 2005;26:1423.
[25] Bras AR, Viciosa MT, Wang Y, Dionísio M, Mano JF. Macromolecules 2006;39:6513.
[26] Weyer S, Hensel A, Schick C. Thermochim Acta 1997;305:267.
[27] Ling X, Spruiell J. J Polym Sci Polym Phys Ed 2006;44:3200.
[28] Kobayashi J, Asahi T, Ichiki M, Oikawa A, Suzuki H, Watanabe T, et al. J Appl Phys 1995;77:2957.
[29] Jaffe M, Wunderlich B. Colloid Polym Sci 1967;216:203.
[30] Minakov A, Mordvintsev D, Schick C. Polymer 2004;45:3755.
[31] Fischer EW, Sterzel HJ, Wegner G. Kolloid Z Z Polym 1973;251:980.
[32] Lefort R, De Gusseme A, Willart JF, Danede F, Descamps M. Int J Pharm 2004;280:209.
[33] Menczel J, Wunderlich B. J Polym Sci Polym Lett 1981;1:261.
[34] El-Taweel SH, Hohne GWH, Mansour AA, Stoll B, Seliger H. Polymer 2004;45:983.
[35] Picciochi R, Wang Y, Alves NM, Mano JF. Colloid Polym Sci 2007;285:575.
[36] Sargsyan A, Tonoyan A, Davtyan S, Schick C. Eur Polym J 2007;43:3113.
[37] Schick C, Donth E. Phys Scr 1991;43:423.
[38] Tran TA, Saïd S, Grohens Y. Macromolecules 2005;38:3867.
[39] Mano JF. J Non Cryst Solids 2007;353:2567.